Proceedings of the 21st International Conference on Global Research and Education (Inter-Academia 2024)

Digital Image Correlation to Assess Residual Strains in WAAM-CMT Manufactured Specimens

D. Budiakivska[a], P. Połaski[b], A. Styk[a,*], D. Golański[b] and M. Kujawińska[a]

[a] *Faculty of Mechatronics, Institute of Micromechanics and Photonics, Warsaw University of Technology, św. A. Boboli 8, 02-525 Warsaw, Poland*
[b] *Faculty of Mechanical and Industrial Engineering, Institute of Manufacturing Technologies, Warsaw University of Technology, Narbutta 85, 02-524 Warsaw, Poland*

Doi: 10.12693/APhysPolA.146.536 *e-mail: adam.styk@pw.edu.pl

The wire arc additive manufacturing with cold metal transfer (WAAM-CMT) technique is one of the 3D printing methods that enables the manufacturing and repairing of complex 3D metal structures. However, the physical processes occurring during WAAM-CMT are challenging to model as they depend on multiple technological parameters such as the material used, welding current, voltage, wire feed rate, travel speed, and cooling. One of the important drawbacks of this technique is the introduction of residual strains into the produced structures. The experimental methodology for determining residual strains in samples manufactured on substrates with different thicknesses is examined to optimise the process and minimise residual strains. The method employs 3D digital image correlation to measure strains released during the stepwise unloading of samples produced on pre-clamped substrates. Example experiments were conducted for 316L stainless steel samples with two different substrate thicknesses. The evaluated data were correlated with technological parameters, potentially identifying optimal WAAM-CMT parameters. Moreover, the results were compared to the finite element method model of the manufacturing process to gain a deeper understanding of the physical processes and to improve finite element method modelling. This hybrid approach helps to identify key technological parameters and plan cooling strategies to minimise residual stresses in WAAM structures.

topics: digital image correlation (DIC), wire arc additive manufacturing (WAAM), residual strains measurements

1. Introduction

Residual stress is the stress that remains in a material after being manufactured, processed, or exposed to external loads. These stresses can significantly affect the material's mechanical properties, durability, and performance. Understanding and measuring residual stress is crucial in engineering applications to ensure structural integrity and reliability. Optical measuring techniques are often employed for this purpose due to their non-destructive nature, high precision, and capability to provide detailed stress profiles.

Residual stresses arise during manufacturing processes like welding, casting, and machining, or through service conditions such as load cycling. They can be beneficial, as in the case of compressive residual stresses introduced by shot peening, or detrimental, leading to crack initiation and propagation.

Accurate measurement of residual stress is vital for predicting the life and performance of components, especially in critical applications such as aerospace, automotive, and structural engineering. It helps in the validation of manufacturing processes, quality control, and in the development of repair strategies.

Currently, the main techniques utilised for residual stress measurement can be divided into destructive and non-destructive. Destructive testing results in damaging the sample or removing a section of material, meaning that the specimen may no longer be used. Among the destructive methods, traditional ones can be mentioned, like slitting and measuring the elongation [1], centre-hole or ring core drilling [2] combined with strain gauges or optical methods (*digital image correlation* (DIC), grating interferometry, *electronic speckle pattern interferometry* (ESPI)) [3] and contour method supported by *finite element method* (FEM) [4].

Among the non-destructive techniques, neutron diffraction [5], synchrotron diffraction, and mostly X-ray diffraction ($\sin^2(\psi)$ method) [6] are dominating. Other experimental methods that are also worth mentioning are magnetic (Barkhausen noise) [7], acoustic emission [8], and ultrasonic methods [9]. They are fast, reliable and can measure complex shapes. The main disadvantages are specimen size and weight restrictions, high cost, limited access, and the accuracy affected by texture and grain size [10, 11].

Experimental methods are based on displacement measurements in selected areas of the tested material. They enable recording the displacements between an undeformed and deformed element or after releasing stresses formed in the material during manufacturing processes. The values of strains and stresses in the material are determined from the relationships between displacements, strains, and stresses. It is important to emphasize that in each case, the indication obtained from a non-destructive measurement depends on many parameters, only one of which is the sought stress.

2. WAAM-CMT manufacturing

Wire arc additive manufacturing (WAAM) is an advanced manufacturing process that combines traditional welding techniques with rapid prototyping technology to create large metal components layer by layer. This technology is mainly known for its efficiency in fabricating large-scale parts with less material waste compared to traditional subtractive manufacturing methods.

WAAM uses an electric arc, typically from *gas metal arc welding* (GMAW) or tungsten inert gas (TIG) welding, as the heat source to melt metal wire feedstock. The melted metal is deposited layer by layer to build a three-dimensional object (see Fig. 1) [12].

The choice of material, often in wire form, includes steel, aluminium, titanium, and nickel-based alloys. The deposition process involves controlling the path of the welding torch and wire feeder to create successive layers, following a predetermined path based on the CAD model of the part.

Localised heating and uneven cooling during the WAAM process introduce large thermal gradients, causing distortion and residual stresses, which can affect the topology and global integrity of a WAAM component.

3. DIC for residual stress measurement

Digital image correlation (DIC) is a non-contact optical method applied for full-field measurements of the displacement and the deformation of solids.

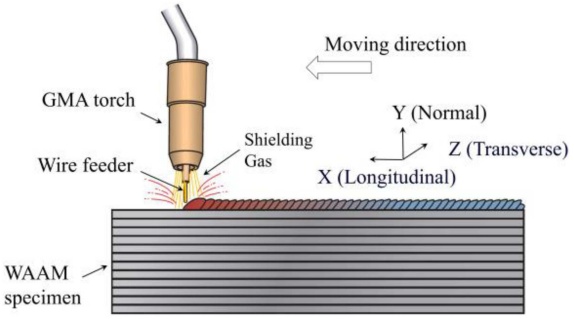

Fig. 1. Diagrammatic sketch of the WAAM process [12].

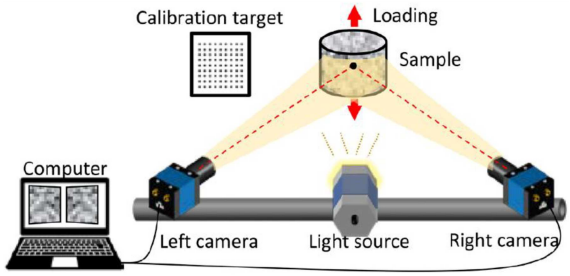

Fig. 2. The scheme of 3D digital image correlation measurement [14].

It uses a sequence of digital images of the sample with a random speckle pattern on its surface. The most significant advantages of this method are the independence of the material of the tested sample and the length-scale of interest [13]. Due to that fact, over the past two decades, the number of various applications of these techniques has rapidly increased [14].

Stereo-DIC, also known as 3D DIC, is a digital image correlation technique used to measure the 3D displacement components and the shape of a sample with various geometries [13].

The calibration of 3D DIC systems is done with flat charts containing a specific grid of markers. During the measurement, a series of image pairs is captured by synchronised cameras. The collected images are then stereo-correlated and triangulated, and the specimen 3D surface shape coordinates for every load are obtained [15]. From that set of objects' 3D shapes, the full displacement vector may be calculated. The scheme of the 3D DIC system is illustrated in Fig. 2 [14].

4. Experiment

During the experimental works, the samples with different process parameters were studied. Two main pre-optimised manufacturing process parameters were considered, namely the welding current

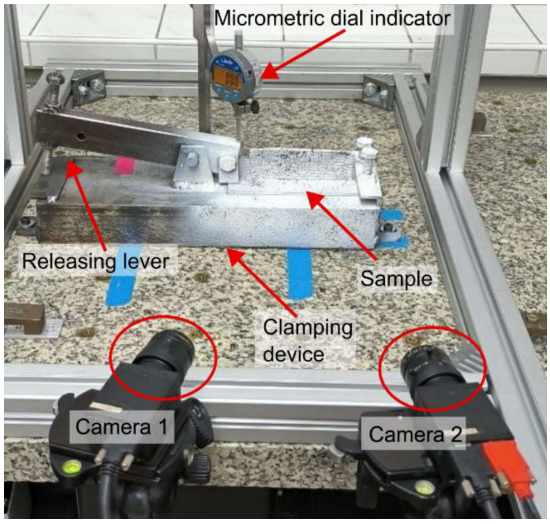

Fig. 3. 3D DIC measurement setup for residual strain measurements.

and the thickness of the base plate on top of which the structure was deposited. A robotic welding station consisting of a *cold metal transfer* (CMT) source, Fronius TPS 2700 and a ZAP-Robotyka IRp-6 robot [16] was used for sample preparation.

The 3D DIC measurement setup for residual strain measurements is presented in Fig. 3. It consists of two cameras (GRAS-50S5M-C Point Grey, 2448 × 2048 pixels, square pixel size of 3.45 μm) mounted rigidly on an aluminium rod and a computer equipped with appropriate software (VIC-3D) for recording and processing of the experimental data. The angle between the cameras was 25.6°. The spatial resolution of the DIC imaging system corresponds to 147 μm with an approximate measurement volume of 200 × 100 × 200 mm^3.

Preparing test samples using WAAM technology required using a substrate made of a material compatible with the deposition material. The applied substrate, namely sheet metal, will partially stiffen the deposit (accumulate stresses), reducing the deformations recorded in the deposit.

To ascertain the influence of substrate thickness on the distribution and magnitude of residual stresses, deposition tests were conducted on substrates with a thickness of 4 and 8 mm, employing constant WAAM process parameters. On each of the plates, models were constructed in the form of vertical walls with a height of approximately 40 mm and a length of 110 mm. The wall thickness was equivalent to a single bead (approximately 4 mm). All of the investigated samples were made of stainless steel 316L. The specific WAAM deposition parameters are detailed in Table I.

The samples were manufactured in a specially prepared holder equipped with a lever mechanism enabling rigid mounting of the substrate plate (at the manufacturing stage) with the possibility of

TABLE I

WAAM deposition test parameters.

No.	Arc voltage [V]	Welding current [A]	Travel speed [mm/s]	Substrate thickness [mm]
1	13.4	78	6.75	8
2	13.4	78	6.75	4

controlled change in the position of the clamp placed at one end of the sample. Upon completion of the manufacturing process, the holder and the finished sample were transferred to the DIC measuring station.

The holder allows the step-wise release of residual stresses from the sample manufactured on the preclamped substrate. The micrometric dial indicator ensures control over the subsequent step determination. The samples were additionally prepared for the measurement by depositing the black and white random pattern.

The measuring station (Fig. 3) was equipped with a digital dial gauge indicating the displacement value caused by the release of stresses accumulated in the sample. Before undertaking the measurement, the sensor reading was set to zero. The DIC measurement was performed each time the sensor reading increased by 0.1 mm. The measurement was completed when the sensor reading did not change (all accumulated stresses were released).

For each WAAM sample measurement, three unloading–loading cycles were performed. During the unloading and loading cycles, the specifically chosen measurement points indicated by the micrometric dial values were tracked. For each measured sample, we have acquired 211 stereo-pairs of images to be further processed in the VIC-3D software. In the processing stage, the maps of displacements in "u", "v", and "w" were calculated. Further, these displacements were used for the calculation of absolute displacement maps, which were applied for comparison with the numerical model. Also, it should be mentioned that we could extract the single point in the displacement map and analyse its displacement variations in time.

The 2D displacement maps calculated for each measured point along the unloading–loading cycle were used to track the changes in displacements that can be correlated with residual strains.

5. Numerical simulation

The studies on assessing residual stresses were also extended to simulation studies. The simulation of the model manufacturing process using the WAAM method and subsequent simulations of the release of accumulated stresses were performed in the Simufact Welding software based on finite

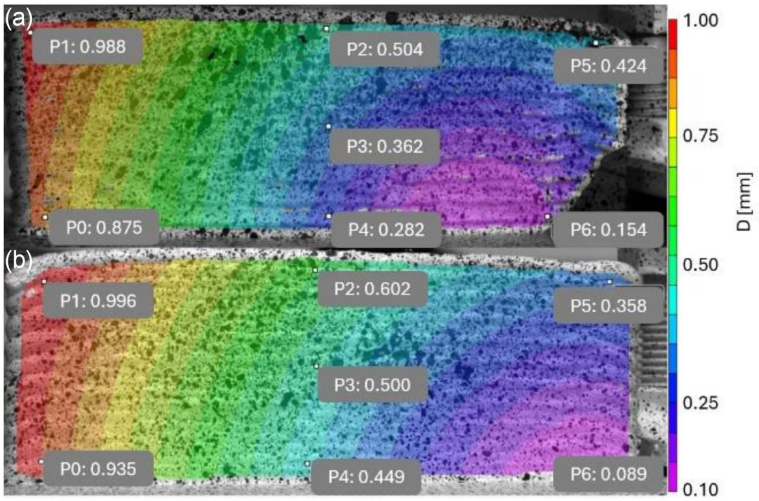

Fig. 4. DIC measurement results distribution of total displacements after releasing all stresses of the sample: (a) on 4 mm substrate, (b) on 8 mm substrate.

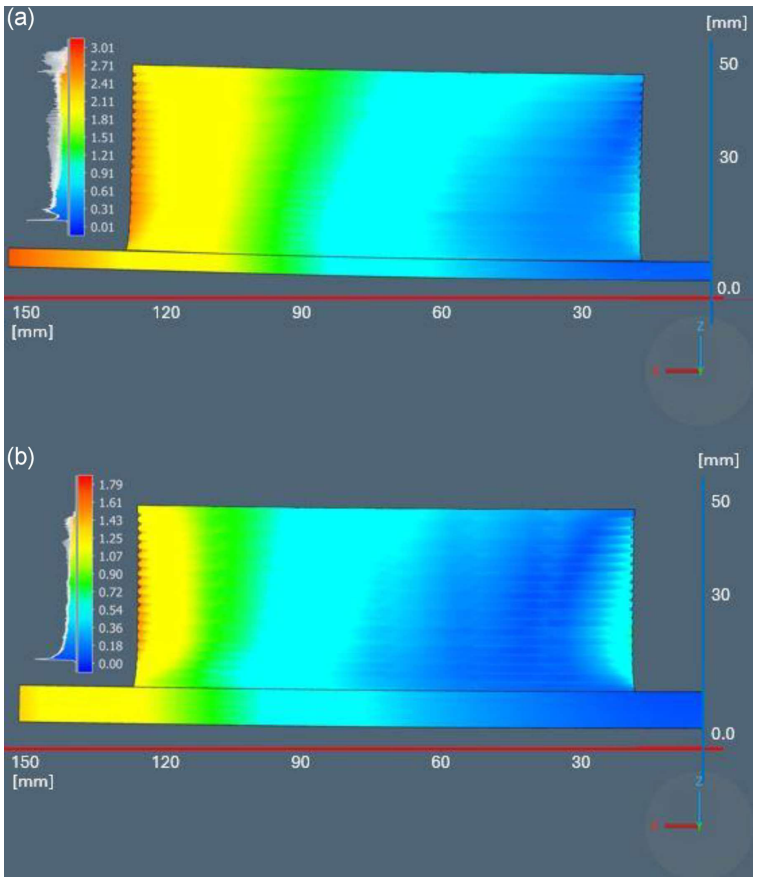

Fig. 5. FEM simulation of distribution of total displacements after releasing all stresses of the sample on the 4 mm (a) and 8 mm (b) substrate.

element method (FEM). This software has a DED (*direct energy deposition*) calculation module dedicated to welding additive manufacturing deposition. The developed model, reflecting the geometry of produced samples, considers the incremental deposition that occurs during the process with a certain degree of approximation to the actual surfacing conditions. In particular, the shape of the sample was simplified (for example, the model surface is flat and not wavy), and the path of the movable support

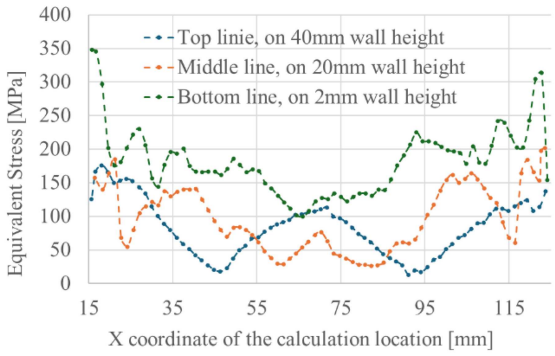

Fig. 6. FEM calculated equivalent stress distribution along the length of the sample for the 8 mm substrate thickness.

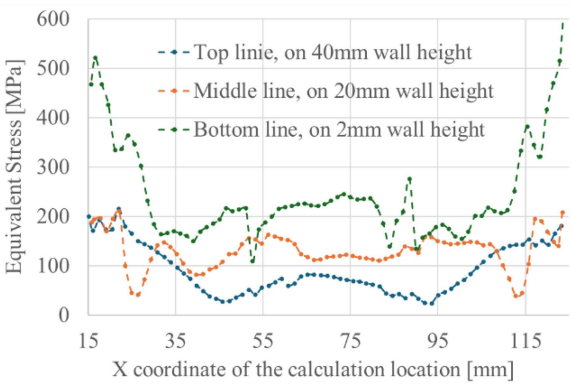

Fig. 7. FEM calculated equivalent stress distribution along the length of the sample for 4 mm substrate thickness.

TABLE II

Calculated $\sigma_{xx,u}$ stresses in samples tested by DIC method.

Substrate thickness [mm]	Maximal stress $\sigma_{xx,u}$ [MPa]	Minimal stress $\sigma_{xx,u}$ [MPa]	Typical stress $\sigma_{xx,u}$ [MPa]
8	1007	−1900	±150 − 400
4	672	−1580	±100 − 400

is, in reality, curvilinear, while the model employs a rectilinear path. Some inaccuracies in numerical calculations may be introduced by the parameters of the heat source used. In the numerical model, a heat source (Goldak model) operating continuously was used, while in reality, in the CMT surfacing device used, heat is introduced to the material in intervals (the electric arc ignites for a moment and then goes out).

6. Results

The results of the total displacement distributions for the samples welded on 8- and 4-mm thick plates are shown in Fig. 4 for the DIC measurements and in Fig. 5 for the FEM simulations, respectively.

In both tests, a similar nature of displacement distribution is visible. The model's left side experiences the largest deformations, which gradually decrease towards the right edge of the sample. In addition, the substrate bending is visible after the surfacing process and due to stress release by controlled release of the sample holder clamp. The differences in the recorded total displacement values may result from simplifications and assumptions of the calculation model, which did not fully reflect the conditions and phenomena during CMT surfacing, which were mentioned earlier. In the case of the FEM model, significantly larger displacements for sample 2 (on a 4 mm substrate) are the result of the lower stiffness of the substrate, which is more susceptible to plastic deformation. The displacements of the model during unloading are the result of releasing the accumulated stresses created during the manufacturing process. Releasing the sample from the holder does not mean releasing all the internal stresses of the sample material.

Figures 6 and 7 show the distribution of equivalent stresses calculated using the FEM method for samples made on 8- and 4-mm thick substrates. The samples show a similar trend of stress distribution. The closer to the substrate plate, the higher the calculated stresses. The lowest stresses were observed near the centre of the sample and in the area of the last applied layer.

The increase in stresses in the substrate area may be caused by a geometric notch at the contact between the substrate plate and the weld. Over most of the sample length, stresses reach values of up to 200–250 MPa. However, at the sample edges, near the substrate, they increase to ≈ 300 and 500 MPa, which may be the effect of stress singularity in this area (that often accompanies FEM calculations).

In the case of the digital image correlation, where the results are in the form of displacements and strains, it is possible to determine stresses in the plane of the produced wall using the relationship between strains and stresses for a plane stress state (longitudinal stress), i.e.,

$$\sigma_{xx,u} = \frac{E}{(1-\nu^2)}\,(\varepsilon_{xx} + \nu\,\varepsilon_{yy}). \tag{1}$$

Table II presents the minimum, maximum, and typical values of the longitudinal stress component σ_{xx} determined from DIC measurements for the obtained strains ε_{xx} and ε_{yy}, assuming data for 316L steel (Young's modulus $E = 193$ GPa, Poisson's ratio $\nu = 0.25$). Most of the calculated stresses σ_{xx}, both tensile and compressive, were in the range of 150–400 MPa, which reflects the stress values determined during the numerical simulation.

7. Conclusions

Using 3D DIC for the determination of displacements and strains during residual stress release provided a lot of valuable data, which should enable the development of a proper FEM model of residual stresses created under various processing parameters and sample materials.

The measurement system can be enhanced by introducing additional 3D DIC systems to monitor eventual base and clamping device displacements and by better defining the unloading point.

The σ_{xx} stresses derived from measured strains using the adopted DIC technique were mainly within the range of 150–400 MPa, both tensile and compressive. In contrast, the stresses calculated using the finite element method (FEM) analysis exhibited lower values, typically within the range of 50 to 200 MPa. This indicates that the stresses within the simulation model were not fully released, as evidenced by the reduced deformation values observed in the model.

The WAAM deposition performed on the thinner 4 mm substrate revealed elevated stress levels compared to those observed for the 8 mm substrate, mainly in the region close to the substrate plate. This phenomenon can be attributed to the reduced thermal capacity of the thinner substrate plate, which experiences a more rapid and intense heating process due to the concentrated heat source. This, in turn, gives rise to an elevated degree of deformation in the resulting sample.

It can be observed that the stresses within the sample wall diminish as the distance from the substrate plate increases. Furthermore, these values remain within a similar range (30–150 MPa) for varying substrate thicknesses.

Although the results of numerical calculations do not differ significantly from those obtained in the DIC tests, the analyses that were conducted indicate the need for further modification of the model. The FEM model has to be significantly enhanced, i.e., (i) for determination of displacements in agreement to sample measurements and (ii) for residual stresses determination, the differences in local material constants should be checked, as well as (iii) the model clamping conditions with releasing stress after finishing deposition of all layers.

It is important to note that the element produced on the substrate plate through the use of the WAAM method should ultimately be detached from the substrate itself. This process should be accompanied by further release of some of the accumulated stresses from the area where the surfacing process was initiated.

References

[1] W. Cheng, I. Finnie, *Residual Stress Measurement and the Slitting Method*, Springer, New York 2006.

[2] M.M. Shokrieh, A.R. Ghanei Mohammadi, in: *Residual Stresses in Composite Materials*, Ed. M.M. Shokrieh, Woodhead Publishing, 2014, p. 15.

[3] M. Kujawińska, L. Sałbut, in: *Handbook of Moire Measurement*, Ed. C.A. Walker, IOP, Bristol 2003.

[4] T. Mishurova, B. Sydow, T. Thiede, I. Sizova, A. Ulbricht, M. Bambach, G. Bruno, *Metals* **10**, 701 (2020).

[5] B. Ahmad, X. Zhang, H. Guo, M.E. Flitzpatrick, L. MacHado, S.C. Neto, S. Williams, *Metals* **12**, 253 (2022).

[6] U. Welzel, J. Ligot, P. Lamparter, A.C. Vermeulen, E.J. Mittemeijer, *J. Appl. Cryst.* **38**, 1 (2005).

[7] D.M. Stewart, K.J. Stevens, A.B. Kaiser, *Curr. Appl. Phys.* **4**, 308 (2004).

[8] S. Sathish, T.J. Moran, R.W. Martin, R. Reibel, *Mater. Sci. Eng. A.* **399**, 84 (2005).

[9] C. Xu, W. Song, Q. Pan, H. Li, S. Liu, *Phys. Proc.* **70**, 594 (2015).

[10] M.E. Fitzpatrick, A. Lodini, *Analysis of Residual Stress by Diffraction using Neutron and Synchrotron Radiation*, CRC Press, London 2003.

[11] M.K. Khan, M.E. Fitzpatrick, S.V. Hainsworth, A.D. Evans, L. Edwards, *Acta Mater.* **59**, 7508 (2011).

[12] H. Abusalma, H. Eisazadeh, F. Hejripour, J. Bunn, D.K. Aidun, *J. Manuf. Process.* **75**, 863 (2022).

[13] E.M.C. Jones, M.A. Iadicola, *A Good Practices Guide for Digital Image Correlation*, International Digital Image Correlation Society, 2018.

[14] B. Pan, *Meas. Sci. Technol.* **29**, 082001 (2018).

[15] VIC-3D 7, Correlated Solutions, Inc., 2016.

[16] P. Połaski, D. Golański, P. Kołodziejczak, A. Pakuła, *Adv. Sci. Technol. Res. J.* (2024).